

Rapid Microwave Preparation and Composition Tuning of the High-Performance Magnetocalorics $(\text{Mn,Fe})_2(\text{P,Si})$

Jason H. Grebenkemper,[†] Joshua D. Bocarsly,^{†,‡} Emily E. Levin,^{†,‡} Gareth Seward,[§] Colin Heikes,[⊥] Craig Brown,[⊥] Sumohan Misra,[#] Fabian Seeler,[#] Kerstin Schierle-Arndt,[#] Stephen D. Wilson,^{†,‡} and Ram Seshadri^{*,†,‡,||}

[†]Materials Research Laboratory, [‡]Materials Department, [§]Department of Earth Science, and ^{||}Department of Chemistry and Biochemistry, University of California, Santa Barbara, California 93106, United States

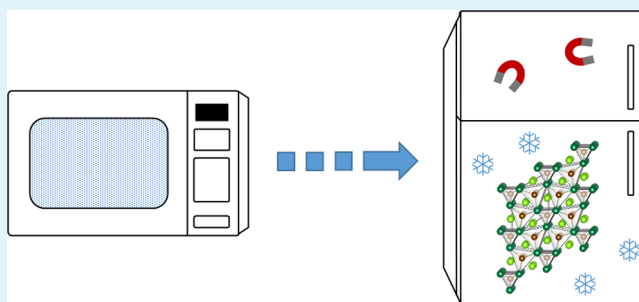
[⊥]Center for Neutron Research, National Institute of Standards and Technology, Gaithersburg, Maryland 20899, United States

[#]BASF SE, 67056 Ludwigshafen, Germany

Supporting Information

ABSTRACT: Rapid preparation utilizing assisted microwave heating permits significantly shorter preparation times for magnetocaloric compounds in the $(\text{Mn,Fe})_2(\text{P,Si})$ family, specifically samples of $(\text{Mn,Fe})_{2-\delta}\text{P}_{0.5}\text{Si}_{0.5}$ with starting compositions of $\delta = 0, 0.06,$ and 0.12 . To fully understand the effects of processing and composition changes on structure and properties, these materials are characterized using synchrotron powder diffraction, neutron powder diffraction, electron microprobe analysis (EMPA), X-ray fluorescence (XRF), and magnetic measurements. The diffraction analysis reveals that increasing δ results in decreasing amounts of the common Heusler $(\text{Mn,Fe})_3\text{Si}$ secondary phase. EMPA shows $(\text{Mn,Fe})_2(\text{P,Si})$ in all three samples to be Mn and P rich, whereas XRF demonstrates that the bulk material is Mn rich yet P deficient. Increasing δ brings the Mn/Fe and P/Si ratios closer to their starting values. Measurements of magnetic properties show an increase in saturation magnetization and ordering temperature with increasing δ , consistent with the increase in Fe and Si contents. Increasing δ also results in a decrease in thermal hysteresis and an increase in magnetic entropy change, the latter reaching values close to what have been previously reported on samples that take much longer to prepare.

KEYWORDS: magnetocaloric materials, microwave synthesis, synchrotron diffraction, neutron diffraction



INTRODUCTION

Although gas compression refrigeration is a mature technology, new cooling methods such as magnetic refrigeration have the potential to exceed current efficiencies obtained from vapor-compression refrigeration without the use of environmentally harmful coolants.¹ Magnetic refrigeration is based on the magnetocaloric effect, where the entropy change that occurs when a material transitions between magnetic states manifests as a change in temperature. To be useful for refrigeration and cooling, a magnetocaloric material should magnetically order near the working temperature, have minimal thermal hysteresis (ΔT_{hys}), and have a large adiabatic temperature change (ΔT_{ad}) and magnetic entropy change (ΔS_{M}) under a moderate applied field (1–2 T).^{2,3}

Some of the most promising magnetocaloric materials come from the Fe_2P structure type.⁴ Fe_2P has a first-order magnetoelastic transition in which the moments ferromagnetically order with an accompanying abrupt change in the dimensions of the unit cell, but no change in structural symmetry.^{5–7} By substitution of Mn for Fe, and As, Ge, or Si for P, a large ΔS_{M} can be achieved at this transition and the

materials can be tuned for optimal magnetocaloric performance.^{8–15} Due to the toxicity of As and the limited supply of Ge, the most likely material to see adoption for widespread cooling applications is $(\text{Mn,Fe})_2(\text{P,Si})$, which forms the hexagonal Fe_2P structure with Si concentrations between 0.24 and 0.5 when Fe and Mn are present in equal amounts.^{16,17} This material can be optimized by adjusting the Mn/Fe and P/Si ratios.^{18,19} Increasing the Fe content leads to an increase in T_{C} , ΔT_{hys} , and ΔS_{M} , whereas increasing the Si content results in a decrease in ΔS_{M} and ΔT_{hys} and an increase in T_{C} .^{20–23} Properties can also be tuned by adjusting the metal to nonmetal ratio, and there are many examples in the literature of materials with compositions of $(\text{Mn,Fe})_{1.95}(\text{P,Si})$.^{21,24–26} Recent work by Fries et al. suggests that the metal to nonmetal ratio has a significant impact on magnetic properties and is closely related to the formation of the $(\text{Mn,Fe})_3\text{Si}$ secondary phase.²⁷ It has also been shown that changes in processing

Received: November 7, 2017

Accepted: February 6, 2018

Published: February 19, 2018

parameters, such as annealing temperature and time, can have a significant impact on the magnetic properties.^{28,29} Due to the large amount of potential configurations available for this material, parametric studies of single degrees of freedom are necessary for tuning the material for magnetocaloric applications.

Current methods for preparing $(\text{Mn,Fe})_2(\text{P,Si})$ are time consuming, often involving long periods of ball milling and high-temperature heat treatment.^{19,22} We have developed a rapid preparation for $(\text{Mn,Fe})_2(\text{P,Si})$ utilizing high-energy ball milling, assisted microwave heating, and brief furnace annealing, allowing materials to be prepared in less than a day. Assisted microwave heating has been successfully used to rapidly prepare high-quality materials for various applications including thermoelectrics, phosphors, and catalysis.^{30–32} Microwave preparations have the benefit of not only reduced reaction times (minutes instead of days), but also decreased energy costs compared to using high-temperature furnaces. Microwave heating also has the advantage of volumetric heating, where the entire material is uniformly and rapidly heated, in contrast to conventional heating, where there is a heat gradient between the exterior of the material and the center.³³

This study investigates the impact of reducing the total metal content on composition, structure, and magnetism in $(\text{Mn}_{0.5}\text{Fe}_{0.5})_{2-\delta}\text{P}_{0.5}\text{Si}_{0.5}$ with $\delta = 0, 0.06, \text{ and } 0.12$ using this new method. Starting Mn/Fe and P/Si ratios were maintained at 1 to separate their influence on properties. Because the nominal composition is unlikely to match the actual composition postreaction, elemental analysis was performed using electron microprobe analysis (EMPA) and X-ray fluorescence (XRF) spectrometry. Combined with detailed phase and structural analyzes from neutron and synchrotron powder diffraction, this gives a detailed picture of the compositional and structural changes caused by reducing the metal content in this preparation.

METHODS

Starting materials representative of precursors used in industrial production were provided by BASF: MnP (97.3%), Mn pieces (99.2%, cleaned by heating at 1000 °C for 12 h in an evacuated fused silica tube), Fe powder (99.5%, -70 mesh), and Si powder (99.7%, -70 mesh). Five gram samples of $(\text{Mn}_{0.5}\text{Fe}_{0.5})_{2-\delta}\text{P}_{0.5}\text{Si}_{0.5}$ ($\delta = 0, 0.06, 0.12$) were prepared by ball milling stoichiometric amounts of the starting materials, corrected for their purities, in a 55 mL tungsten carbide vial with two 11.2 mm tungsten carbide balls using a SPEX 8000M Mixer/Mill for 30 min. The ball-milled powder was then hand ground using an agate mortar and pestle until it was homogeneous, pressed into a 13 mm pellet, and sealed under 1/4 atm Ar in a fused silica tube. The base of the ampoule was inserted into a 20 mL alumina crucible filled with 6 g of activated charcoal (DARCO 12–20 mesh) and placed in a cylindrical cavity carved into an alumina fiberboard block and covered with another piece of fiberboard. This enclosure was placed off-center on the rotating plate of a domestic microwave oven (Panasonic NN-SN651B, 1200 W) and heated at 360 W for 20 min. The pellet was removed from the ampoule after cooling and sealed in a new fused silica tube under vacuum. The evacuated ampoule was then placed in a furnace at 1100 °C for 2 h, followed by a water quench. This heat treatment is necessary for achieving a sharp magnetic transition (see Figure S2, Supporting Information).

High-resolution synchrotron powder diffraction data were collected using beamline 11-BM at the Advanced Photon Source (APS), Argonne National Laboratory, using an average wavelength of 0.414536 Å. Discrete detectors covering an angular range from -6 to 16° 2θ were scanned over a 34° 2θ range, with data points collected every 0.001° 2θ and a scan speed of 0.01° s^{-1} .

Neutron powder diffraction data were collected using the BT-1 32 detector neutron powder diffractometer at the NIST Center for Neutron Research (NCNR). The samples were loaded in a vanadium sample can of length 50 mm and diameter 6.0 mm. Data were collected under ambient conditions. A Cu(311) monochromator with a $\lambda = 1.5403(2)$ Å and in-pile collimation of 60 min of arc were used. Data were collected over the range of 3–168° 2θ with a step size of 0.05°.

Joint Rietveld refinements of the neutron and synchrotron diffraction data were performed using TOPAS 6. Unit cell parameters were allowed to freely refine for each data set, whereas atomic positions, occupancies, and thermal parameters were corefined. Total compositions were constrained to values determined from EMPA. P/Si occupancies were fixed assuming a uniform distribution of both elements across the two distinct crystallographic sites. Peaks from the $\delta = 0.12$ neutron powder diffraction data that had significant magnetic contributions were excluded from the refinement to reduce their impact on Mn and Fe occupancies.

Elemental compositions were obtained using electron microprobe for the majority $(\text{Mn,Fe})_2(\text{P,Si})$ phases and X-ray fluorescence for the bulk material. Electron microprobe analyses were performed on pieces of each annealed pellet using a Cameca SX100 equipped with five wavelength dispersive spectrometers (WDSs). The same pieces were analyzed by X-ray fluorescence on Rigaku Primus IV using semiquantitative analysis, where three points were analyzed across each sample with a spot size of 1 mm.

Magnetic measurements were performed using a Quantum Design Dynacool Physical Properties Measurement System equipped with a vibrating sample magnetometer. Magnetization versus temperature data were collected using a sweep rate of 1 K min^{-1} with an applied field of 2 T, and magnetization versus field loops were collected at 100 K from -5 to 5 T. Values of magnetic entropy change (ΔS_M) were determined from magnetic measurements using the Maxwell relation

$$\left(\frac{\partial S}{\partial H}\right)_T = \left(\frac{\partial M}{\partial T}\right)_H \quad (1)$$

where H is the applied field and M is magnetization. This relation gives the following equation for determining ΔS_M

$$\Delta S_M(H, T) = \int_0^H \left(\frac{\partial M}{\partial T}\right)_{H'} dH' \quad (2)$$

Temperature derivatives were calculated from smoothed magnetization versus temperature traces collected at magnetic fields ranging from 0.1 to 5 T and integrated with respect to field.

RESULTS AND DISCUSSION

Preparations of $(\text{Mn,Fe})_2(\text{P,Si})$ were confirmed using synchrotron powder diffraction, shown in Figure 1. Although the majority phase of all three compositions is hexagonal $(\text{Mn,Fe})_2(\text{P,Si})$, these samples also contain Heusler $(\text{Mn,Fe})_3\text{Si}$ and cristobalite (SiO_2) impurities. Two distinct $(\text{Mn,Fe})_2(\text{P,Si})$ phases with the same space group but different lattice parameters are observed in the $\delta = 0.12$ diffraction pattern due to phase coexistence near the magnetoelastic transition. These phases are referred to as low temperature (LT) for the magnetically ordered phase and high temperature (HT) for the paramagnetic phase. This is only seen in the $\delta = 0.12$ sample because the others order below room temperature. Neutron powder diffraction patterns are shown in Figure 2.

Joint Rietveld refinements were performed using the synchrotron and neutron powder diffraction data. The patterns are well fit as a combination of HT, LT, Heusler, and cristobalite. Unit cell parameters taken from the refined synchrotron HT $(\text{Mn,Fe})_2(\text{P,Si})$ phase are shown in Figure 3 and Table 1. As δ increases, a increases, whereas c decreases. As

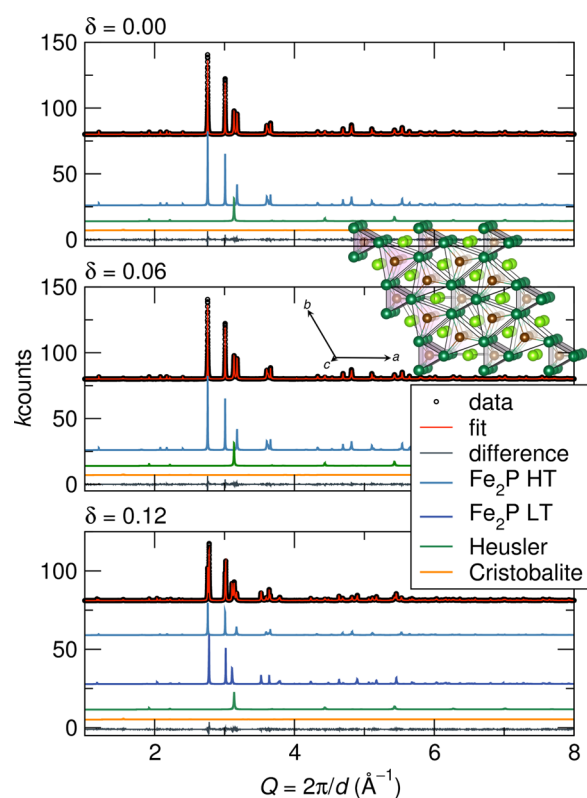


Figure 1. Synchrotron X-ray powder diffraction patterns of $(\text{Mn}_{0.5}\text{Fe}_{0.5})_{2-\delta}\text{P}_{0.5}\text{Si}_{0.5}$ taken at 300 K and Rietveld fits to that data, showing individual contributions for the impurity phases: Heusler $(\text{Mn,Fe})_3\text{Si}$ and cristobalite SiO_2 . The inset displays a view of the Fe_2P structure of the materials discussed here, depicted as P-centered prisms formed by the transition metals.

a result of these changes, the c/a ratio decreases as δ increases and the overall volume increases. This agrees with that of previous studies where increasing Si content results in c decreasing, whereas a and the volume increase; however, the opposite trend has been observed for increasing Fe content.^{17,22} The overall trend following the change in Si content is however not unexpected considering that the change in Si content is significantly larger than the change in Fe content. Lattice parameter, a , for the Heusler $\text{Fe}_{3-x}\text{Mn}_x\text{Si}$ varies from 5.66900(5) to 5.66530(4) Å for $\delta = 0$ and 0.12, respectively, suggesting a composition range of $x \approx 1.25$ – 1.05 .³⁴

The refined weight fractions of each phase are shown in Figure 4a. The amount of cristobalite remains constant at roughly 2% in each material and could be due to devitrification of the silica tube. As δ increases, the amount of $(\text{Mn,Fe})_3\text{Si}$ decreases, with a corresponding increase in $(\text{Mn,Fe})_2(\text{P,Si})$. Occupancies determined from the joint refinements are presented in Figure 4b. Mn occupancies for both sites decrease with increasing δ , whereas Fe occupancies increase.

Electron microprobe X-ray maps (Figure 5) reveal porous materials consisting of uniform $(\text{Mn,Fe})_2(\text{P,Si})$ majority phases and inclusions of $(\text{Mn,Fe})_3\text{Si}$ on the order of 20 μm . Elemental compositions were determined for the majority phases using EMPA and for the bulk using XRF, both shown in Figure 6. Despite starting with equal ratios of Fe/Mn, all samples are Mn rich in both the bulk and $(\text{Mn,Fe})_2(\text{P,Si})$. Although both the bulk and $(\text{Mn,Fe})_2(\text{P,Si})$ are Fe deficient, the bulk material contains more Fe than the $(\text{Mn,Fe})_2(\text{P,Si})$ phase due to the additional Fe content in the $(\text{Mn,Fe})_3\text{Si}$ impurity phase. In the

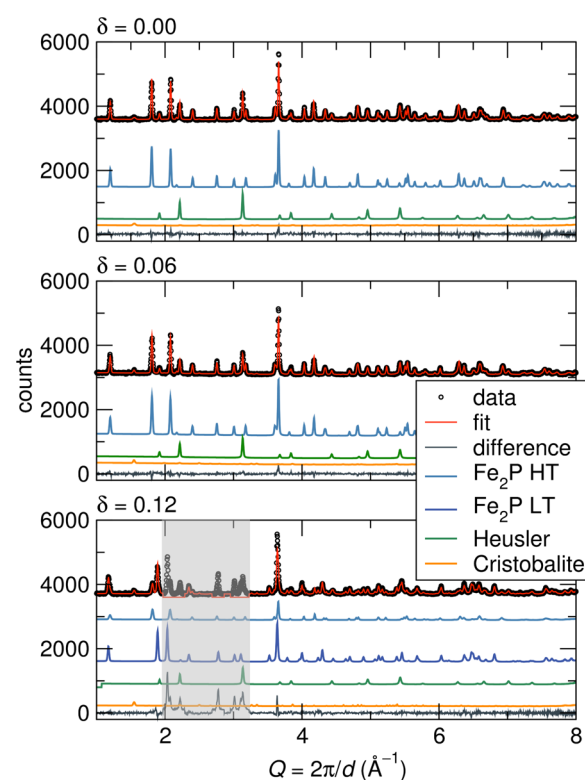


Figure 2. Neutron powder diffraction patterns of $(\text{Mn}_{0.5}\text{Fe}_{0.5})_{2-\delta}\text{P}_{0.5}\text{Si}_{0.5}$ taken at 300 K and Rietveld fits to that data, showing individual contributions for the Heusler and cristobalite impurity phases. Peaks with significant magnetic contributions have been masked in $\delta = 0.12$.

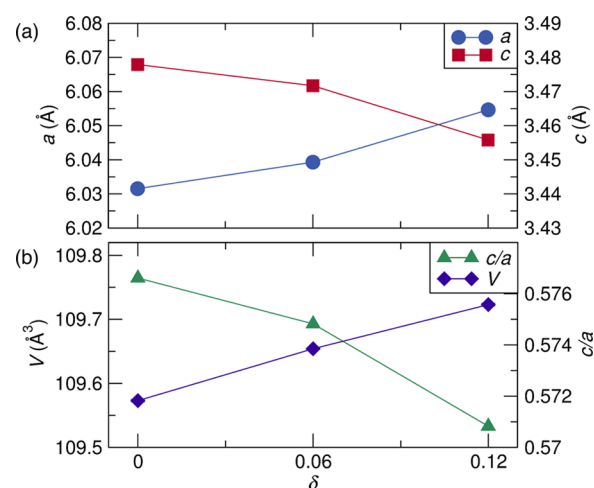
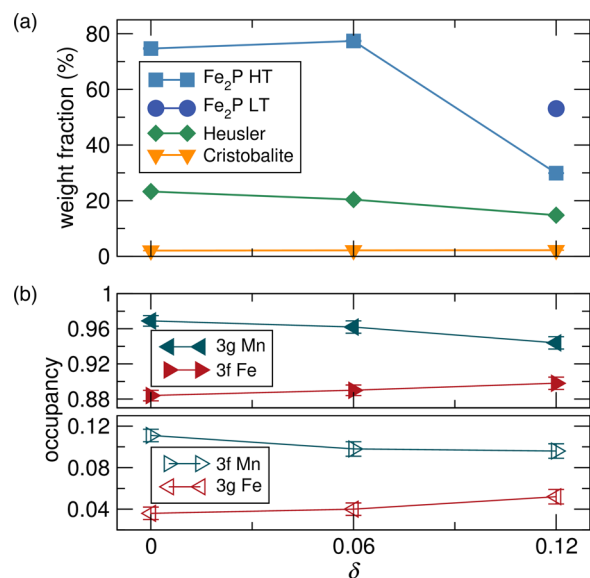
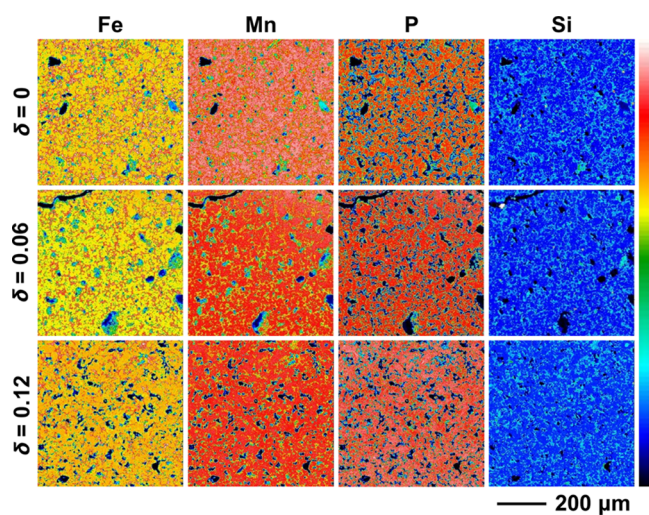


Figure 3. Unit cell parameters (a) a and c and (b) unit cell volume and c/a ratio for $(\text{Mn}_{0.5}\text{Fe}_{0.5})_{2-\delta}\text{P}_{0.5}\text{Si}_{0.5}$ determined from Rietveld refinements of synchrotron powder diffraction data.

case of P and Si, which also started with equal ratios, $(\text{Mn,Fe})_2(\text{P,Si})$ is P rich, whereas the bulk material is Si rich. This can again be attributed to $(\text{Mn,Fe})_3\text{Si}$, which does not contain any P. As δ is increased, the Fe/Mn and P/Si ratios move closer to their starting values. Elemental formulas for the majority phases of $\delta = 0$, 0.06, and 0.12 were determined from EMPA to be $\text{Mn}_{1.10(3)}\text{Fe}_{0.933(6)}\text{P}_{0.61(1)}\text{Si}_{0.39(1)}$, $\text{Mn}_{1.06(5)}\text{Fe}_{0.934(4)}\text{P}_{0.57(3)}\text{Si}_{0.43(3)}$, and $\text{Mn}_{1.04(2)}\text{Fe}_{0.95(2)}\text{P}_{0.55(1)}\text{Si}_{0.45(1)}$, respectively. Despite starting with compositions that were metal deficient,

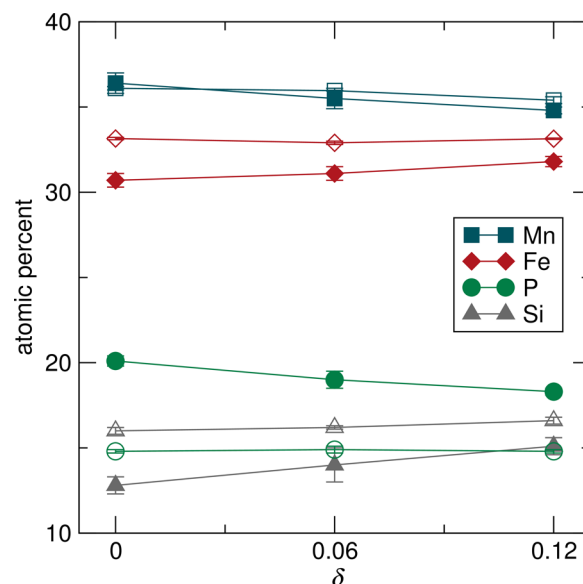
Table 1. Unit Cell Parameters Taken from Synchrotron Rietveld Refinements and Occupancies and Impurity Weight Fractions of $(\text{Mn}_{0.5}\text{Fe}_{0.5})_{2-\delta}\text{P}_{0.5}\text{Si}_{0.5}$ Taken from Joint Neutron and Synchrotron Rietveld Refinements

δ	R_{wp} (%)	a (Å)	c (Å)	vol (\AA^3)	3f Fe occ	3f Mn occ	3g Mn occ	3g Fe occ	(Mn,Fe) ₃ Si (wt %)	SiO ₂ (wt %)
0	15.90	6.03153(3)	3.47789(3)	109.572(2)	0.884(6)	0.111(6)	0.969(6)	0.036(6)	23.3(2)	2.07(6)
0.06	12.11	6.03929(3)	3.47151(2)	109.653(1)	0.890(6)	0.098(7)	0.962(7)	0.040(6)	20.4(2)	2.16(4)
0.12	10.82	6.05463(4)	3.45616(4)	109.723(2)	0.898(7)	0.096(7)	0.944(7)	0.052(7)	14.8(2)	2.22(3)

**Figure 4.** (a) Weight fractions of LT and HT $(\text{Mn,Fe})_2(\text{P,Si})$, and the $(\text{Mn,Fe})_3\text{Si}$ and cristobalite impurities, and (b) Mn/Fe site occupancies of $(\text{Mn}_{0.5}\text{Fe}_{0.5})_{2-\delta}\text{P}_{0.5}\text{Si}_{0.5}$ as determined by joint synchrotron and neutron Rietveld refinements.**Figure 5.** Electron microprobe X-ray backscatter maps of annealed pellets of $(\text{Mn}_{0.5}\text{Fe}_{0.5})_{2-\delta}\text{P}_{0.5}\text{Si}_{0.5}$. The color scale shows the relative weight percents of each element.

these materials do not appear to have $(\text{Mn,Fe})/(\text{P,Si})$ ratios significantly below 2:1, with the $\delta = 0.12$ sample displaying a ratio of 1.99:1, within error of 2:1.

Key values from magnetization data are listed in Table 2. Field-dependent magnetization measurements, shown in Figure 7a, reveal an increase in saturation magnetization with increasing δ . This is consistent with the increasing Fe and Si contents.^{18,35} No hysteresis with respect to field is observed for any of the studied materials. Figure 7b shows temperature-

**Figure 6.** Elemental compositions of $(\text{Mn}_{0.5}\text{Fe}_{0.5})_{2-\delta}\text{P}_{0.5}\text{Si}_{0.5}$ as determined from EMPA (filled markers) and XRF (empty markers).

dependent magnetization taken at 2 T. Increasing δ leads to an increase in magnetic ordering temperature and a decrease in thermal hysteresis. This increase in T_C can be attributed to the increase in Fe and Si contents, as increasing amounts of either element will result in higher ordering temperatures.^{20,22} In the case of thermal hysteresis, increasing Si content has been reported to decrease ΔT_{hys} , whereas increasing Fe content should increase it.²⁰ The Heusler impurity $\text{Fe}_{3-x}\text{Mn}_x\text{Si}$ ferromagnetically orders around 202(2)–181(1) K for compositions from 1.05 to 1.25 and has been found to exhibit a very small magnetocaloric effect.^{34,36} As this ordering temperature range is below the $(\text{Mn,Fe})_2(\text{P,Si})$ transitions in this study, this impurity is expected to have a minimal impact on the observed magnetism.

Figure 8 shows ΔS_M calculated from magnetization measurements. Increasing δ leads to an increase in ΔS_M , reaching the highest value for the $\delta = 0.12$ sample with $-20 \text{ J kg}^{-1} \text{ K}^{-1}$ at 290 K and a 5 T field. Increasing Si content is expected to result in a decrease in ΔS_M , whereas increasing Fe content increases it.^{21,23} Despite the contradictory effects of increasing Fe and Si contents, ΔS_M increases by a significant amount with increasing δ , which cannot be solely attributed to the increase in the weight fraction of $(\text{Mn,Fe})_2(\text{P,Si})$.

CONCLUSIONS

Samples of $(\text{Mn}_{0.5}\text{Fe}_{0.5})_{2-\delta}\text{P}_{0.5}\text{Si}_{0.5}$ ($\delta = 0, 0.06, 0.12$) were successfully prepared by assisted microwave heating of ball-milled powders. Characterization by powder diffraction revealed the impurities $(\text{Mn,Fe})_3\text{Si}$ and cristobalite. Despite starting 1:1 ratios for Mn/Fe and P/Si, $(\text{Mn,Fe})_2(\text{P,Si})$ was Fe and Si deficient in all samples due to the occurrence of $(\text{Mn,Fe})_3\text{Si}$ impurities. Increasing δ does not actually result in a

Table 2. Magnetic Properties of $(\text{Mn}_{0.5}\text{Fe}_{0.5})_{2-\delta}\text{P}_{0.5}\text{Si}_{0.5}$

δ	T_C (K)	μ_{sat} (μ_B)	μ_{sat} (μ_B) ^a	ΔS_M ($\text{J kg}^{-1} \text{K}^{-1}$)		ΔS_M ($\text{J kg}^{-1} \text{K}^{-1}$) ^a		ΔT_{hys} (K) ^b
				$H = 2$ T	$H = 5$ T	$H = 2$ T	$H = 5$ T	
0	224	3.1	4.2	-6.0	-15.2	-8.0	-20.4	48
0.06	260	3.3	4.3	-6.8	-17.1	-8.8	-22.1	35
0.12	302	3.7	4.5	-8.2	-20.0	-9.9	-24.1	27

^aCorrected using Fe_2P weight percent from Rietveld refinement. ^bMeasured using a ramp rate of 1 K min^{-1} .

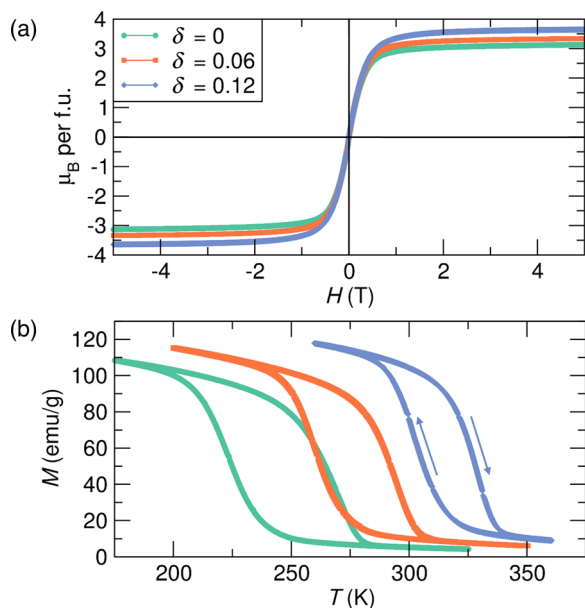


Figure 7. (a) Field-dependent magnetization taken at 100 K and (b) temperature-dependent magnetization data taken at $H = 2$ T of $(\text{Mn}_{0.5}\text{Fe}_{0.5})_{2-\delta}\text{P}_{0.5}\text{Si}_{0.5}$. The arrows indicate heating and cooling for the two branches of temperature-dependent data.

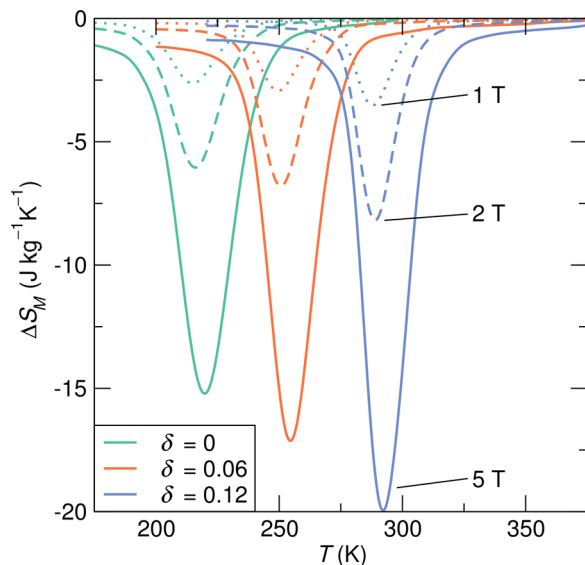


Figure 8. ΔS_M for select fields of $(\text{Mn}_{0.5}\text{Fe}_{0.5})_{2-\delta}\text{P}_{0.5}\text{Si}_{0.5}$ as obtained using eq 1 with temperature-dependent magnetization data collected at several fields.

change in the metal to nonmetal ratio but instead causes a decrease in the amount of the $(\text{Mn,Fe})_3\text{Si}$ impurity and an increase in Fe and Si contents in $(\text{Mn,Fe})_2(\text{P,Si})$. This leads to a contraction of c and an expansion of a and unit cell volume,

consistent with the increasing Si content but contradictory to the increasing Fe content. Magnetization measurements were also consistent with the increase in Fe and Si contents, with saturation magnetization and T_C increasing with increasing δ . Whereas increasing Fe and Si contents have contradictory effects on thermal hysteresis, increasing δ leads to a decrease in ΔT_{hys} , consistent with increasing Si content. The opposite is observed in ΔS_M , where increasing δ results in a larger ΔS_M , consistent with increasing Fe content.

On the basis of the effects of reducing the total metal content in these microwave preparations, it is expected that further increasing δ could be used to decrease the amount of $(\text{Mn,Fe})_3\text{Si}$ and bring the final composition of $(\text{Mn,Fe})_2(\text{P,Si})$ to be more in line with the initial Mn/Fe and P/Si ratios. Although this would likely further boost ΔS_M , it would also increase the T_C even further, potentially bringing it far above the desired region near 300 K that is ideal for common cooling applications. By tuning metal deficiency along with Mn/Fe and P/Si ratios, an optimized material could be produced using this rapid preparation.

■ ASSOCIATED CONTENT

Supporting Information

The Supporting Information is available free of charge on the ACS Publications website at DOI: 10.1021/acsami.7b16988.

X-ray diffraction and magnetization data for a sample after the microwave step; temperature-dependent magnetization data used to calculate ΔS_M for $(\text{Mn}_{0.5}\text{Fe}_{0.5})_{2-\delta}\text{P}_{0.5}\text{Si}_{0.5}$ ($\delta = 0, 0.06, 0.12$) (PDF)

■ AUTHOR INFORMATION

Corresponding Author

*E-mail: seshadri@mrl.ucsb.edu.

ORCID

Jason H. Grebenkemper: 0000-0001-7236-1874

Ram Seshadri: 0000-0001-5858-4027

Notes

The authors declare no competing financial interest.

■ ACKNOWLEDGMENTS

This work was supported by BASF Corporation through the California Research Alliance (CARA, Award No. 040543) and the National Science Foundation under DMR-SSMC 1710638. J.D.B. is supported by the National Science Foundation Graduate Research Fellowship Program under grant number 1650114. The research reported here made use of shared facilities of the UCSB MRSEC (NSF DMR 1720256), a member of the Materials Research Facilities Network (www.mrfn.org). Use of the Advanced Photon Source at Argonne National Laboratory was supported by the U.S. Department of Energy, Office of Science, Office of Basic Energy Sciences, under Contract No. DE-AC02-06CH11357. We thank the

National Institute of Standards and Technology, U.S. Department of Commerce, in providing the neutron research facilities used in this work.

REFERENCES

- (1) Franco, V.; Blázquez, J.; Ingale, B.; Conde, A. The Magneto-caloric Effect and Magnetic Refrigeration Near Room Temperature: Materials and Models. *Annu. Rev. Mater. Res.* **2012**, *42*, 305–342.
- (2) Brown, G. V. Magnetic heat pumping near room temperature. *J. Appl. Phys.* **1976**, *47*, 3673–3680.
- (3) Gómez, J. R.; García, R. f.; de Miguel Catoira, A.; Gómez, M. r. Magnetocaloric effect: A review of the thermodynamic cycles in magnetic refrigeration. *Renewable Sustainable Energy Rev.* **2013**, *17*, 74–82.
- (4) Rundqvist, S.; Jellinek, F.; Magnéli, A.; Andersson, G.; Stenhagen, E.; Palmstierna, H. The Structures of $\text{Ni}_6\text{Si}_2\text{B}$, Fe_2P and Related Phases. *Acta Chem. Scand.* **1959**, *13*, 425–432.
- (5) Wäppling, R.; Häggström, L.; et al. First order magnetic transition, magnetic structure, and vacancy distribution in Fe_2P . *J. Solid State Chem.* **1975**, *13*, 258–271.
- (6) Lundgren, L.; Tarmohamed, G.; Beckman, O.; Carlsson, B.; Rundqvist, S. First Order Magnetic Phase Transition in Fe_2P . *Phys. Scr.* **1978**, *17*, 39–48.
- (7) Delczeg-Czirjak, E. K.; Pereiro, M.; Bergqvist, L.; Kvashnin, Y. O.; di Marco, I.; Li, G.; Vitos, L.; Eriksson, O. Origin of the magnetostructural coupling in $\text{FeMnP}_{0.75}\text{Si}_{0.25}$. *Phys. Rev. B* **2014**, *90*, No. 214436.
- (8) Tegus, O.; Brück, E.; Buschow, K. H. J.; de Boer, F. R. Transition-metal-based magnetic refrigerants for room-temperature applications. *Nature* **2002**, *415*, 150–152.
- (9) Brück, E.; Tegus, O.; Zhang, L.; Li, X.; de Boer, F.; Buschow, K. Magnetic refrigeration near room temperature with Fe_2P -based compounds. *J. Alloys Compd.* **2004**, *383*, 32–36.
- (10) Yibole, H.; Guillou, F.; Zhang, L.; van Dijk, N. H.; Brück, E. Direct measurement of the magnetocaloric effect in $\text{MnFe}(\text{P},\text{X})$ ($\text{X} = \text{As}, \text{Ge}, \text{Si}$) materials. *J. Phys. D: Appl. Phys.* **2014**, *47*, No. 075002.
- (11) Liu, D.; Yue, M.; Zhang, J.; McQueen, T. M.; Lynn, J. W.; Wang, X.; Chen, Y.; Li, J.; Cava, R. J.; Liu, X.; Altounian, Z.; Huang, Q. Origin and tuning of the magnetocaloric effect in the magnetic refrigerant $\text{Mn}_{1-x}\text{Fe}_{0.9}\text{(P}_{0.8}\text{Ge}_{0.2})$. *Phys. Rev. B* **2009**, *79*, No. 014435.
- (12) Trung, N. T.; Ou, Z. Q.; Gortenmulder, T. J.; Tegus, O.; Buschow, K. H. J.; Brück, E. Tunable thermal hysteresis in $\text{MnFe}(\text{P},\text{Ge})$ compounds. *Appl. Phys. Lett.* **2009**, *94*, No. 102513.
- (13) Delczeg-Czirjak, E. K.; Delczeg, L.; Punkkinen, M. P. J.; Johansson, B.; Eriksson, O.; Vitos, L. Ab initio study of structural and magnetic properties of Si-doped Fe_2P . *Phys. Rev. B* **2010**, *82*, No. 085103.
- (14) Song, L.; Wang, G.; Ou, Z.; Haschaolu, O.; Tegus, O.; Brück, E.; Buschow, K. Magnetic properties and magnetocaloric effect of $\text{MnFeP}_{0.5}\text{Ge}_{0.5-x}\text{Si}_x$ compounds. *J. Alloys Compd.* **2009**, *474*, 388–390.
- (15) Brück, E.; Tegus, O.; Thanh, D. T. C.; Trung, N. T.; Buschow, K. H. J. A review on Mn based materials for magnetic refrigeration: Structure and properties. *Int. J. Refrig.* **2008**, *31*, 763–770.
- (16) Zhang, L.; Može, O.; Prokeš, K.; Tegus, O.; Brück, E. Neutron diffraction study of history dependence in $\text{MnFeP}_{0.6}\text{Si}_{0.4}$. *J. Magn. Mater.* **2005**, *290–291*, 679–681.
- (17) Höglin, V.; Cedervall, J.; Andersson, M. S.; Sarkar, T.; Hudl, M.; Nordblad, P.; Andersson, Y.; Sahlberg, M. Phase diagram, structures and magnetism of the $\text{FeMnP}_{1-x}\text{Si}_x$ -system. *RSC Adv.* **2015**, *5*, 8278–8284.
- (18) Cam Thanh, D. T.; Brück, E.; Trung, N. T.; Klaasse, J. C. P.; Buschow, K. H. J.; Ou, Z. Q.; Tegus, O.; Caron, L. Structure, magnetism, and magnetocaloric properties of $\text{MnFeP}_{1-x}\text{Si}_x$ compounds. *J. Appl. Phys.* **2008**, *103*, No. 07B318.
- (19) Höglin, V.; Hudl, M.; Sahlberg, M.; Nordblad, P.; Beran, P.; Andersson, Y. The crystal and magnetic structure of the magnetocaloric compound $\text{FeMnP}_{0.5}\text{Si}_{0.5}$. *J. Solid State Chem.* **2011**, *184*, 2434–2438.
- (20) Dung, N. H.; Ou, Z. Q.; Caron, L.; Zhang, L.; Thanh, D. T. C.; de Wijs, G. A.; de Groot, R. A.; Buschow, K. H. J.; Brück, E. Mixed magnetism for refrigeration and energy conversion. *Adv. Energy Mater.* **2011**, *1*, 1215–1219.
- (21) Dung, N. H.; Zhang, L.; Ou, Z. Q.; Brück, E. From first-order magneto-elastic to magneto-structural transition in $(\text{Mn},\text{Fe})_{1.95}\text{P}_{0.50}\text{Si}_{0.50}$ compounds. *Appl. Phys. Lett.* **2011**, *99*, No. 092511.
- (22) He, A.; Svitlyk, V.; Mozharivskiy, Y. Synthetic Approach for $(\text{Mn},\text{Fe})_2(\text{Si},\text{P})$ Magnetocaloric Materials: Purity, Structural, Magnetic, and Magnetocaloric Properties. *Inorg. Chem.* **2017**, *56*, 2827–2833.
- (23) Katagiri, K.; Nakamura, K.; Wada, H. Magnetocaloric properties and magnetic refrigerant capacity of $\text{MnFeP}_{1-x}\text{Si}_x$. *J. Alloys Compd.* **2013**, *553*, 286–290.
- (24) Carlsson, B.; Gölin, M.; Rundqvist, S. Determination of the homogeneity range and refinement of the crystal structure of Fe_2P . *J. Solid State Chem.* **1973**, *8*, 57–67.
- (25) Dung, N. H.; Zhang, L.; Ou, Z. Q.; Brück, E. Magnetoelastic coupling and magnetocaloric effect in hexagonal Mn-Fe-P-Si compounds. *Scr. Mater.* **2012**, *67*, 975–978.
- (26) Ou, Z.; Zhang, L.; Dung, N.; van Eijck, L.; Mulders, A.; Avdeev, M.; van Dijk, N.; Brück, E. Neutron diffraction study on the magnetic structure of Fe_2P -based $\text{Mn}_{0.66}\text{Fe}_{1.29}\text{P}_{1-x}\text{Si}_x$ melt-spun ribbons. *J. Magn. Mater.* **2013**, *340*, 80–85.
- (27) Fries, M.; Pfeuffer, L.; Bruder, E.; Gottschall, T.; Ener, S.; Diop, L. V.; Gröb, T.; Skokov, K. P.; Gutfleisch, O. Microstructural and magnetic properties of Mn-Fe-P-Si (Fe_2P -type) magnetocaloric compounds. *Acta Mater.* **2017**, *132*, 222–229.
- (28) Thang, N. V.; Yibole, H.; van Dijk, N. H.; Brück, E. Effect of heat treatment conditions on $\text{MnFe}(\text{P},\text{Si},\text{B})$ compounds for room-temperature magnetic refrigeration. *J. Alloys Compd.* **2017**, *699*, 633–637.
- (29) Lai, J. W.; Zheng, Z. G.; Huang, B. W.; Yu, H. Y.; Qiu, Z. G.; Mao, Y. L.; Zhang, S.; Xiao, F. M.; Zeng, D. C.; Goubitz, K.; Brück, E. Microstructure formation and magnetocaloric effect of the Fe_2P -type phase in $(\text{Mn},\text{Fe})_2(\text{P}, \text{Si}, \text{B})$ alloys. *J. Alloys Compd.* **2018**, *735*, 2567–2573.
- (30) Birkel, C. S.; Douglas, J. E.; Lettiere, B. R.; Seward, G.; Verma, N.; Zhang, Y.; Pollock, T. M.; Seshadri, R.; Stucky, G. D. Improving the thermoelectric properties of half-Heusler TiNiSn through inclusion of a second full-Heusler phase: microwave preparation and spark plasma sintering of $\text{TiNi}_{1+x}\text{Sn}$. *Phys. Chem. Chem. Phys.* **2013**, *15*, 6990–6997.
- (31) Brgoch, J.; Borg, C. K. H.; Denault, K. A.; Douglas, J. R.; Amanda Strom, T.; Denbaars, S. P.; Seshadri, R. Rapid microwave preparation of cerium-substituted sodium yttrium silicate phosphors for solid state white lighting. *Solid State Sci.* **2013**, *26*, 115–120.
- (32) Misch, L. M.; Brgoch, J.; Birkel, A.; Mates, T. E.; Stucky, G. D.; Seshadri, R. Rapid Microwave Preparation and ab Initio Studies of the Stability of the Complex Noble Metal Oxides $\text{La}_2\text{BaPdO}_5$ and $\text{La}_2\text{BaPtO}_5$. *Inorg. Chem.* **2014**, *53*, 2628–2634.
- (33) Bhattacharya, M.; Basak, T. A review on the susceptor assisted microwave processing of materials. *Energy* **2016**, *97*, 306–338.
- (34) Yoon, S.; Booth, J. G. Magnetic properties and structures of some ordered $(\text{FeMn})_3\text{Si}$ alloys. *J. Phys. F: Met. Phys.* **1977**, *7*, 1079–1095.
- (35) Dung, N. H.; Zhang, L.; Ou, Z. Q.; Zhao, L.; van Eijck, L.; Mulders, A. M.; Avdeev, M.; Suard, E.; van Dijk, N. H.; Brück, E. High/low-moment phase transition in hexagonal Mn-Fe-P-Si compounds. *Phys. Rev. B* **2012**, *86*, No. 045134.
- (36) Bocarsly, J. D.; Levin, E. E.; Garcia, C. A. C.; Schwennicke, K.; Wilson, S. D.; Seshadri, R. A simple computational proxy for screening magnetocaloric compounds. *Chem. Mater.* **2017**, *29*, 1613–1622.